2013-09-01

Rabbit anti-HIV-1 monoclonal antibodies raised by immunization can mimic the antigen-binding modes of antibodies derived from HIV-1-infected humans

Ruimin Pan
New York University School of Medicine

Et al.

JVI Journals.ASM.org

Rabbit Anti-HIV-1 Monoclonal Antibodies Raised by Immunization Can Mimic the Antigen-Binding Modes of Antibodies Derived from HIV-1-Infected Humans

Ruimin Pan,[a] Jared M. Sampson,[a] Yuxin Chen,[b] Michael Vaine,[b] Shixia Wang,[b] Shan Lu,[b] Xiang-Peng Kong[a]

Department of Biochemistry and Molecular Pharmacology, New York University School of Medicine, New York, New York, USA[a]; Department of Medicine, University of Massachusetts Medical School, Worcester, Massachusetts, USA[b]

The rabbit is a commonly used animal model in studying antibody responses in HIV/AIDS vaccine development. However, no rabbit monoclonal antibodies (MAbs) have been developed previously to study the epitope-specific antibody responses against HIV-1 envelope (Env) glycoproteins, and little is known about how the rabbit immune system can mimic the human immune system in eliciting such antibodies. Here we present structural analyses of two rabbit MAbs, R56 and R20, against the third variable region (V3) of HIV-1 gp120. R56 recognizes the well-studied immunogenic region in the V3 crown, while R20 targets a less-studied region at the C terminus of V3. By comparison of the Fab/epitope complex structures of these two antibodies raised by immunization with that of the corresponding human antibodies derived from patients chronically infected with HIV-1, we found that rabbit antibodies can recognize immunogenic regions of gp120 and mimic the binding modes of human antibodies. This result can provide new insight into the use of the rabbit as an animal model in AIDS vaccine development.

Animal models are indispensable in the development of HIV/AIDS vaccines. A comparison of the structure and function of monoclonal antibodies (MAbs) derived from animal models with MAbs derived from human patients will tell us (i) how animal immune systems mimic the human immune system in humoral responses and (ii) how animal antibodies derived by immunization differ from antibodies derived from chronically infected patients. This information will help us to optimize vaccine designs. The rabbit is a unique animal model with many advantages. First, rabbits are known to be able to produce high-affinity antibodies against molecules that may not be immunogenic to mice, another commonly used animal model (1). Second, studies have suggested that the rabbit immune system is more similar to the immune systems of primates and humans than to that of mice (2–5). Third, rabbit immunoglobulin loci have been well characterized and are relatively simple (1, 6, 7). In addition, rabbits can produce antibodies with a long complementarity-determining region (CDR) 3 in the heavy chain or CDR H3 (5), a property often found in potent human anti-HIV gp120 MAbs (8). Finally, rabbits, unlike mice, can provide a sufficient amount of serum for evaluation by neutralization and other assays.

Rabbit antibodies have certain unique features (1). For the light chains, there are four common allotypes, b4, b5, b6, and b9, all belonging to the kappa-1 gene family. For the heavy chain, about 80 to 90% use a VH1 germ line gene with diversity derived from gene conversion and somatic hypermutations (9). The three major heavy-chain allotypes, a1, a2, and a3, differ in frame regions 1 and 3. Even though the rabbit heavy chain has limited combinatory possibilities, rabbits are still able to produce a diverse set of kappa genes for the light chain, resulting in antibodies with a broad range of diversity (10). Interestingly, there is a unique interdomain disulfide bond linking the variable and constant domains of the kappa light chain, usually between residues 80 (Kabat numbering; 11) and 170 (residue 171 in the previous literature) and less frequently between residues 108 and 170 (12, 13). This disulfide bond was suggested to help increase the stability of rabbit antibodies for a long shelf life (1).

We have carried out an extensive HIV/AIDS vaccine study using rabbits as the animal model and have generated a panel of rabbit MAbs that provide a unique opportunity to study their structures by protein crystallography (62). Here we present structural analyses of two rabbit MAbs against the third variable region (V3) of HIV-1 gp120. V3 plays a key role in virus entry into the host cell, participating in the binding of the CCR5 or CXCR4 coreceptor (14–17). V3 is about 35 amino acids in length, and the structure of full-length V3 in the context of the gp120 core showed that it can be divided into three regions, the base in the gp120 core (residues 296 to 300 and 326 to 331), the flexible stem (residues 301 to 303 and 319 to 325), and the crown at the distal apex (304 to 318) (18, 19). The V3 crown can be further divided into three smaller regions, the arch of the beta hairpin of the V3 crown (consisting of residues 312 to 315), the band (residues 304 to 305 and 317 to 318), and the circlet between the arch and the band, which is more genetically diverse than the other two regions (19). The amino acid sequence of the arch is often GPGR in clade B strains and GPGQ in non-clade B strains.

There are many anti-V3 MAbs derived from human patients, as well as from animal models other than the rabbit (20–24). Most of the known anti-V3 MAbs are against the V3 crown; only a few of them target the C-terminal region, including a mouse MAb raised by immunization with a synthetic peptide (25). Several recently described highly potent human MAbs, including PGT128, are also against the C-terminal region of V3, as well as its associ-

Received 28 March 2013 **Accepted** 7 July 2013
Published ahead of print 17 July 2013
Address correspondence to Xiang-Peng Kong, xiangpeng.kong@med.nyu.edu.

doi:10.1128/JVI.00843-13

ated glycans (26). Many of the anti-V3 MABs are characterized by structural methods, including protein crystallography and the nuclear magnetic resonance (NMR) method (19, 27–40). These structural studies of MAbs against the V3 crown showed that they have, in general, two antigen-binding modes. (i) In the "ladle" mode, the antibodies have a long CDR H3 (the handle of the ladle) interacting with the main chain of the N-terminal beta strand of the V3 crown and a pocket at the base of the CDR H3 (the bowl of the ladle) interacting with the apex beta turn of the V3 crown. (ii) In the "cradle" mode, the antigen lies along a long binding groove resembling a cradle (19, 38, 39). The former is represented by human MAb 447-52D, and the latter is represented by several human MAbs, including MAb 2557, encoded by the IGHV5-51 genes (19, 38).

We present here several Fab/epitope complex structures of rabbit anti-V3 MAbs R56 and R20 that had been raised by immunization with gp120 of clade B strain JR-FL by using the DNA prime-protein boost regimen (41). The epitopes of R56 and R20 have been mapped to the V3 crown and the V3 C-terminal region, respectively. R56 has been shown to neutralize SF162 and MW965.26, and it also neutralizes ss1196, QH0692, and bal.26 with modest activities, but R20 does not neutralize the strains tested (62). By analyzing the antigen-antibody interactions of these MAbs and comparing them with those of human and mouse anti-V3 antibodies, we showed that immunization of rabbits with HIV-1 gp120 can elicit anti-V3 crown antibodies with a binding mode similar to that of human IGHV5-51 antibodies and that this immunization can also produce rabbit antibodies that target an epitope in the C-terminal region that overlaps the epitope of human MAb PGT128.

MATERIALS AND METHODS

Fab production and purification. Rabbit MAbs R56 and R20 were derived from a New Zealand White rabbit immunized with gp120 of clade B strain JR-FL by using a DNA prime-protein boost regimen, and hybridoma production was carried out by a contracted service (Epitomics, Burlingame, CA) (62). Epitope mapping by using overlapping peptides of gp120 showed that the epitope of R56 is at the crown of gp120 V3, while that of R20 is in the C-terminal region of V3. The details of the production and antigenicity characterization of these and related MAbs will be published separately (62). The Fab fragments of R56 and R20 were prepared by papain digestion as described previously (38). Briefly, the IgG molecules were mixed with papain at a 20:1 molar ratio and 100 mM Tris (pH 6.8) with 1 mM cysteine hydrochloride and 4 mM EDTA. The mixture was incubated for 1 h at 37°C, and the reaction was stopped by adding 10 mM iodoacetamide. The Fab molecules were separated from the Fc fragments and the undigested IgG by protein A affinity chromatography, further purified by size exclusion chromatography, and concentrated to 10 mg/ml for crystallization.

Crystallization, data collection, structure determination and refinement. For R56, we have crystallized the Fab with two V3 peptides, one derived from HIV-1 strain JR-FL ($V3_{JR-FL}$ [NNTRKSIHIG PGRAFY TTGE IIG], residues 301 to 324 in the HXB2 numbering scheme) and another from the consensus A sequence ($V3_{conA}$ [NNTRKSIRIG PGQAF YATGD IIG], residues 301 to 324). These peptides were synthesized by commercial sources. For R20, we have crystallized the Fab with a peptide derived from the consensus B sequence ($V3_{conB}$ [TTGEIIGDIR QAHCN], residues 319 to 332), and the peptide was obtained from the NIH AIDS Research and Reference Reagent Program (peptide 8842 from the set of HIV-1 consensus subtype B Env [15-mer] peptides). All of the peptides were dissolved in water to a concentration of 10 mg/ml and mixed with the Fab molecules in excess at a 10:1 molar ratio before crystallization by the hanging-drop method. The optimized crystallization condition (well solution) for complexes of Fab R56/V3s is 26% polyethylene glycol (PEG) 6000, 1 M LiCl, and 0.1 M Tris (pH 8.0), while that for the Fab R20/V3 complex is 1.5 M ammonium sulfate, 1.7% PEG 400, 85 mM sodium cacodylate (pH 6.5), and 15% (vol/vol) glycerol. We have also crystallized Fab R20 alone with 1.4 M ammonium sulfate, 1.7% PEG 400, 85 mM HEPES (pH 7.5), and 15% glycerol. For data collection, crystals of Fab R56 complexes were soaked briefly in the crystallization solution with an additional 20% glycerol before being flash frozen in liquid nitrogen, while those of Fab R20 were frozen directly. All X-ray diffraction data sets were collected at beam line X6A, National Synchrotron Light Source (NSLS), Brookhaven National Laboratory, and processed with the HKL2000 software package (42). The structures were determined by molecular replacement with MOLREP in the CCP4 software package (43). The structures of Fab R56 complexes were solved first with a starting model built on a homologous Fab (Protein Data Bank [PDB] accession no. 2X7L), and the Fab structure of R56 was then used as the starting model for Fab R20 structures. Cycles of manual adjustments and refinements of the structures were carried out with COOT and PHENIX (44, 45). The final structural analysis and figure rendering were carried out with the PyMOL and ICM software packages (46, 47) and the web tools PISA (www.ebi.ac.uk/msd-srv/prot_int/pistart.html) for hydrogen bonds and Abnum (www.bioinf.org.uk/abs/abnum/) for application of the Kabat residue-numbering scheme.

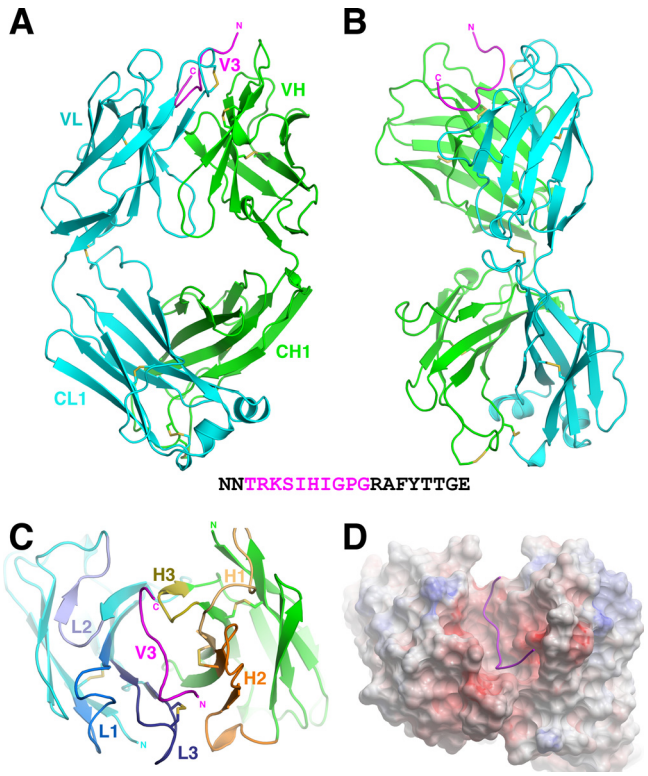

FIG 1 Structure of Fab R56 in complex with $V3_{JR-FL}$. (A) Ribbon representation of a front view of the Fab R56/$V3_{JR-FL}$ complex with the light and heavy chains and the V3 epitope colored cyan, green, and magenta, respectively (a coloring scheme kept throughout this report, except where indicated otherwise). Disulfide bonds are shown by side chain sticks. (B) Side view of the complex. (C) Top view of the complex looking at the antigen-binding site of Fab R56. The CDRs are labeled and colored differently from the rest of the Fab. (D) Surface representation of Fab R56 colored according to its electrostatic surface potentials, with the negatively charged region in red and the positively charged region in blue. V3 is shown as a ribbon. The inset is the sequence of the peptide used for crystallization, and the magenta residues are those visualized in the crystal structure.

TABLE 1 Crystallization data collection and refinement statistics

Parameter	Result(s)[a] for Fab:			
	R56/$V3_{JRFL}$	R56/$V3_{conA}$	R20/$V3_{conB}$	R20/PEG
Data collection				
Space group	$P2_1$	$P2_1$	$P2_12_12_1$	$P2_12_12_1$
Cell dimensions				
a, b, c (Å)	70.51, 74.34, 84.43	69.84, 74.35, 84.96	70.223, 118.977, 134.946	70.649, 119.690, 135.337
α, β, γ (°)	90, 90, 90	90, 90, 90	90, 90, 90	90, 90, 90
Resolution (Å)	2.03 (2.07–2.03)	2.50 (2.54–2.50)	2.60 (2.64–2.60)	2.27 (2.31–2.27)
R_{merge}	8.5 (45.0)	16.1 (58.7)	15.9 (66.4)	10.7 (59.3)
I/σI ratio	18.8 (2.4)	8.9 (2.6)	11.1 (2.7)	22.5 (3.8)
% Completeness	99.5 (94.2)	93.7 (89.9)	97.6 (95.4)	99.9 (99.5)
Redundancy	4.2 (3.8)	3.9 (4.0)	5.7 (5.6)	8.2 (8.1)
Refinement				
Resolution (Å)	36.23–2.03	26.46–2.50	38.05–2.60	38.27–2.27
No. of reflections	56,014	30,171	34,658	53,548
R_{work}/R_{free} ratio	18.13/22.32	18.95/26.54	18.45/23.45	18.43/22.64
No. of atoms				
Protein	6,447	6,336	6,670	6,566
Solvent	805	479	369	730
B factors				
Protein	27.9	24.11	41.1	29.1
Solvent	34.9	22.08	31.3	34.3
RMSD				
Bond lengths (Å)	0.008	0.008	0.009	0.008
Bond angles (°)	1.168	1.147	1.188	1.088

[a] Values in parentheses are for the outer resolution shell.

Protein structure accession numbers. The atomic coordinates of the structures of the Fab R56/$V3_{JR-FL}$, Fab R56/$V3_{conA}$, Fab R20/$V3_{Cterm}$, and Fab R20/PEG complexes have been deposited in the Research Collaboratory for Structural Bioinformatics PDB and assigned accession numbers 4JO1, 4JO2, 4JO3, and 4JO4, respectively.

RESULTS

Determination of the structures of Fabs R56 and R20. We first determined the crystal structures of Fab R56 in complex with its epitope, which was mapped to the crown region of V3 (Fig. 1 and Table 1). We crystallized Fab R56 in complex with two different V3 peptides, NNTRKSIHIG PGRAFYTTGE IIG ($V3_{JR-FL}$), derived from the clade B strain JR-FL, and NNTRKSIRIG PGQAFY ATGD IIG ($V3_{conA}$), derived from the consensus A sequence of gp120. These two peptides were selected because JR-FL gp120 was the one used to immunize the rabbit and the consensus A sequence has a GPGQ motif in the crown arch, representing non-clade B HIV-1 strains. We determined the Fab R56/$V3_{JR-FL}$ and Fab R56/$V3_{conA}$ complex structures by molecular replacement and refined them to 2.0 Å and 2.5 Å resolutions, respectively (Fig. 1; Table 1). The crystals of both complexes belong to monoclinic space group $P2_1$ with essentially the same unit cell parameters. The two Fab/V3 complexes in the asymmetry unit are highly similar (for example, the root mean square deviation [RMSD] for superimposition of all of the C-α atoms is 0.16 Å in the R56/$V3_{JR-FL}$ complex). We therefore, for simplicity, refer to only one of the complexes. We assigned the chain identities (IDs) L, H, and P, respectively, to the light and heavy chains and the epitope of the first Fab/V3 complex in the asymmetric unit. We numbered the residues of the light and heavy chains by following the Kabat and Wu convention, applied to the coordinates with the Abnum server (48), and the residues of V3 in the HXB2 numbering scheme (49). A residue is referred to by its number preceded by its chain ID, for example, Arg^{P315} refers to arginine residue 315 of the V3 epitope. Although 23-mer peptides were used for crystallization, only 10 residues, from Thr^{P303} to Gly^{P314} of the V3 crown region, with the sequence TRKSIHIGPG for $V3_{JR-FL}$ or TRKSIRIGPG for $V3_{conA}$, were observed in the electron densities and have thus been built into the final structures (Fig. 1). Since the R56/$V3_{conA}$ structure has a slightly twinned data set with a lower resolution (Table 1) and is essentially the same as that of Fab R56/$V3_{JR-FL}$, we have not included it here but the atomic coordinates have been deposited in the PDB.

We then determined the crystal structure of Fab R20 in complex with its epitope, which was mapped to the C-terminal region of V3 (Fig. 2 and Table 1). We crystallized the Fab fragment of R20 in complex with a 15-mer V3 peptide of the consensus B sequence, TTGEIIGDIR QAHCN ($V3_{conB}$). The complex structure was determined by molecular replacement and refined to 2.6 Å resolution (Fig. 2 and Table 1). The crystals belong to the orthorhombic space group $P2_12_12_1$ with two Fab/V3 complexes in the asymmetric unit. Again we refer to only one of the complexes in this report, as the structures of the two complexes are highly similar (RMSD of superimposition of all C-α = 0.55 Å). We have numbered the residues of the Fab R20/V3 complex in the same way as those of

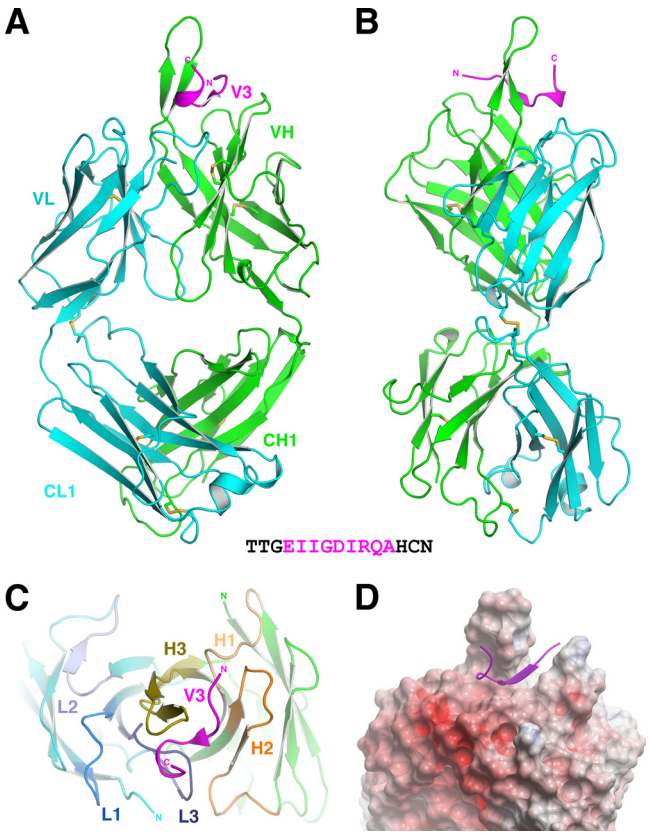

FIG 2 Structure of Fab R20 in complex with $V3_{conB}$. (A) Ribbon representation of a front view the Fab R20/$V3_{conB}$ complex. (B) Side view of the complex. (C) Top view of the complex looking at the antigen-binding site of Fab R20 with the CDRs labeled and colored differently from the rest of the Fab. (D) Surface representation of Fab R20 colored according to its electrostatic surface potentials. The inset is the sequence of the peptide used for crystallization, and the magenta residues are those visualized in the crystal structure.

the R56/V3 complex. Although a 15-mer peptide was used for crystallization, only nine residues, Glu^{P322} to Ala^{P329} of the V3 C-terminal region, with the sequence EIIGDIRQA, were observed. We have also crystallized Fab R20 alone without any peptides and refined the structure to 2.27 Å resolution (Table 1). Interestingly, an elongated PEG molecule from the crystallization condition was found at the same position of the bound V3 epitope in the R20/$V3_{conB}$ complex structure. We have not included the Fab R20/PEG structure here, but the atomic coordinates have been deposited in the PDB.

Overall structural features of rabbit antibodies. Our crystallographic analyses of Fabs R56 and R20 have revealed and explained several salient features of the overall structures of rabbit antibodies.

(i) Structural basis for rabbit heavy-chain allotype recognition. The three major allotypes, a1, a2, and a3, are detectable with antiallotype antisera raised by immunizing rabbits of one type with IgG of another type. The allotype markers are located at the first and third frame regions of the heavy chain. Sequence alignment showed that both R56 and R20 belong to the a3 allotype (Fig. 3A). Thus, the frame regions of Fabs R56 and R20 are highly similar and superimposed well (Fig. 4). Homology structural model building of the VH domains for the a1 and a2 allotypes showed that the surface charges of the first and third frame regions of all three allotypes are substantially different from each other (Fig. 3B to D). Thus, any antibodies that recognize this region of one allotype will not be able to bind the same region of another allotype.

(ii) An interdomain disulfide bond (Fig. 4D and E). Both R56 and R20 have an interdomain disulfide bond in the elbow region of the light chain, linking residue 80 of the variable region (VL) with residue 170 of the first constant region (CL1) (Fig. 4D). This limits the variation of the elbow angles in the antibodies, with 142° for R56 and 154° for R20. Some rabbit antibodies were predicted to have an alternative disulfide bond between residues 108 and 170 (20). Our structures showed that this is possible as the distance between the C-α atoms of these two residues is ~5.6 Å (Fig. 4D), a suitable distance for disulfide bond formation. However, this alternative disulfide bond may have less restriction for the elbow angles in the antibodies.

(iii) Other noncanonical disulfide bonds among the CDR loops. There are two additional noncanonical disulfide bonds in R56 and R20. One is unique to R56 in CDR L3 between Cys^{L94} and Cys^{L95D} (Fig. 4E). This disulfide bond is involved in a van der Waals contact with the hydrophobic residues of the V3 epitope (Fig. 5). A search of the GenBank database found at least three sequences of rabbit light chains with a similar disulfide bond sequence (CSSADC) in CDR L3. We have also observed a similar disulfide bond in CDR H3 of a human antibody (CPGGSC; unpublished), a rare observation in human antibodies. Another noncanonical disulfide bond, present in both R56 and R20, is between Cys^{H35A} and Cys^{H50}, linking CDRs H1 and H2 (Fig. 4E). While this report was being prepared, an uncomplexed structure of the Fab fragment of a rabbit antibody specific for amyloid prefibrillar oligomer appeared in another publication (50) and the light-chain interdomain disulfide bond was discussed there.

Antigen-binding mode of R56. The structures of R56/V3 complexes showed that R56 binds the V3 crown by using the cradle-binding mode (Fig. 1 and 5), similar to that of the human anti-V3 IGHV5-51 MAbs (19, 39). Its antigen-binding site is shaped like a cradle between the light and heavy chains ~14 Å deep and ~10 Å wide with CDR L3 at one end of the cradle and CDR H3 at the other end (Fig. 1C and 5A). Similar to that of the human anti-V3 crown MAbs, the antigen-binding site of R56 has a negative charge contributed in part by three CDR residues from the light chain (Asp^{L50}, Asp^{L93}, and Asp^{L95C}) and three CDR residues from the heavy chain (Asp^{H34}, Glu^{H52}, and Asp^{H101}), all located at the periphery of the cradle. The bottom of the cradle is very hydrophobic and is formed by residues Ala^{L34}, Leu^{L49}, Leu^{L89}, Cys^{L94}, Cys^{L95D}, and Ala^{L96} from the light chain and residues Cys^{H50} and Phe^{H96} from the heavy chain (Fig. 5). The aforementioned two noncanonical disulfide bonds (Cys^{H35A}-Cys^{H50} and Cys^{L94}-Cys^{L95D}) in the CDRs both contribute to this hydrophobic base. Interestingly, the epitope of R56 superimposed well on that of MAb 447-52D (RMSD = 0.75 Å with the superimposed C-α atoms of eight residues [P305 to P314]), even though the latter belongs to the ladle V3-binding mode.

Our Fab R56/V3 complex structures showed that the epitope recognized by R56 consists of 10 amino acids (P303 to P314) in the N-terminal half of the V3 crown (Fig. 1 and 5). The N terminus of the epitope harbors two highly conserved positively charged band residues (Arg^{P304} and Lys^{P305}), and the C terminus ends with the highly conserved Gly^{P312} Pro^{P313} Gly^{P314} sequence of the crown arch. The epitope lies along the cradle with its N terminus sitting

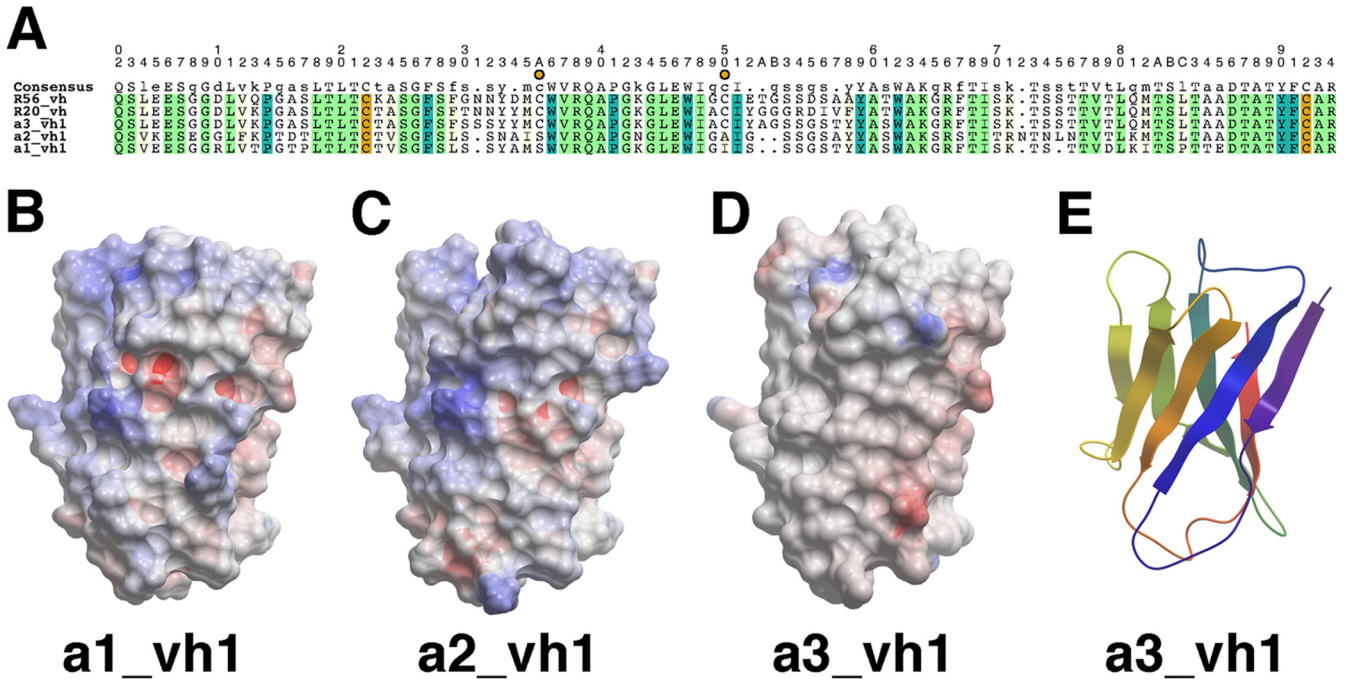

FIG 3 Surface analyses of the three allotypes of rabbit antibodies. (A) Sequence alignment of the heavy-chain Fv regions of R56 and R20 with those of rabbit major heavy-chain germ line allotypes a1, a2, and a3. The intensity of the green color indicates the conservation of the sequence regions. Cysteine residues of the conserved canonical Fv disulfide bond are shaded yellow, and the cysteine residues of the noncanonical disulfide bonds in allotype a3 are indicated by yellow-filled circles above the alignment. Computational modeling of the heavy-chain Fv regions of germ line allotypes a1 and a2 (B and C) on the basis of the structure of R56 (a3) (D). The electrostatic surface potentials of all three allotypes are shown with the allotype marker regions facing forward. (E) The heavy-chain Fv of R56 is shown as a ribbon for a reference. The ribbon is colored from the N terminus (purple) to the C terminus (orange).

on top of the disulfide bond (Cys^{L94}-Cys^{L95D}) of CDR L3 and its C terminus extending toward CDR H3. The antigen-antibody interactions buried a total surface area of 750 $Å^2$ with 356 $Å^2$ from the antibody and 394 $Å^2$ from the epitope. There are three key components of the antigen-antibody interactions (Fig. 5). The first is a salt bridge between band residue Arg^{P304} of the epitope and Asp^{H34} of CDR H1. Negatively charged Glu^{H52} sits on the top of Arg^{P304}, leaving the salt bridge largely buried. The second is the hydrophobic interactions between highly conserved circlet residues Ile^{P307} and Ile^{P309} of the epitope and the hydrophobic base of the antigen-binding site, burying these two isoleucines in the center of the cradle. The third is Pro^{P313} at the GPG beta turn stacking with the side chain of Tyr^{L49} in CDR L2. Interestingly, the side chain of circlet residue His^{P308} (Arg^{P308} in $V3_{conA}$) in the center of the epitope points away from the antibody toward the solvent; thus, it does not contribute to the antigen-antibody interaction. Therefore, R56 does not distinguish the sequence difference between JR-FL and consensus A (data not shown). There are at least two facts explaining the broad reactivity of R56 (62). (i) The interacting residues in the three key components are highly conserved among HIV-1 strains, and (ii) the side chain of variable residue His^{P308}/Arg^{P308} is not involved in the antigen-antibody interaction. It is also clear from the structures that R56 will not be able to bind gp120 of 92UG021, a clade D strain with the sequence VSYRTPIGVG (from 303 to 314) in the epitope region of R56 (62). In particular, the region of the antigen-binding site that fits Ser^{P306} in JR-FL will not be able to accommodate the long side chain of an Arg in the case of 92UG021. Similarly, R56 will not bind gp120 of the MN strain, which also has an Arg at position P306. In addition, R56 does not neutralize commonly used strain IIIB because it has a QR insertion in the V3 crown just before the GPG turn, and Gln has a large side chain, which does not fit the space that is occupied by Gly^{P312} in the JR-FL/conA complex structures.

Antigen-binding mode of R20. R20 has a long CDR H3 of 21 amino acids, unlike R56, which has a short CDR H3 of only 4 amino acids (Kabat definition). CDR H3 of R20 forms a beta hairpin standing tall at the center of its antigen-binding site (Fig. 2). This conformation is similar to that of several human and rhesus MAbs, such as quaternary neutralizing epitope MAbs 2909 and 2.5B (51). Residues at the top of the other CDR loops form a pedestal-like structure. This pedestal is roughly 30 Å long and 10 Å wide and is contributed about equally by the light chain at one end and the heavy chain at the other end. The antigen-binding site of R20 runs across the light chain and heavy chain; this is again different from that of R56, whose antigen-binding site groove is the chasm between the light and heavy chains.

Our Fab R20/$V3_{conB}$ complex structure showed that the epitope recognized by R20 consists of nine amino acids (P322 to P329, including a numbering insertion for Ile^{P322A} in the HXB2 scheme) of the C-terminal region of V3 (Fig. 2 and 6). This epitope is shaped like a fishhook lying on the top of the pedestal of the antigen-binding site. A short two-residue beta strand (Gly^{P324} and Asp^{P326}) in the N-terminal half of the epitope—the shank of the fishhook—forms a parallel beta sheet with the C-terminal strand of the CDR H3 hairpin. This beta-sheet-type interaction is similar to the ladle antigen-binding mode described for anti-V3 MAbs 447-52D and 537 (38). Following the beta strand, a short 3_{10} G

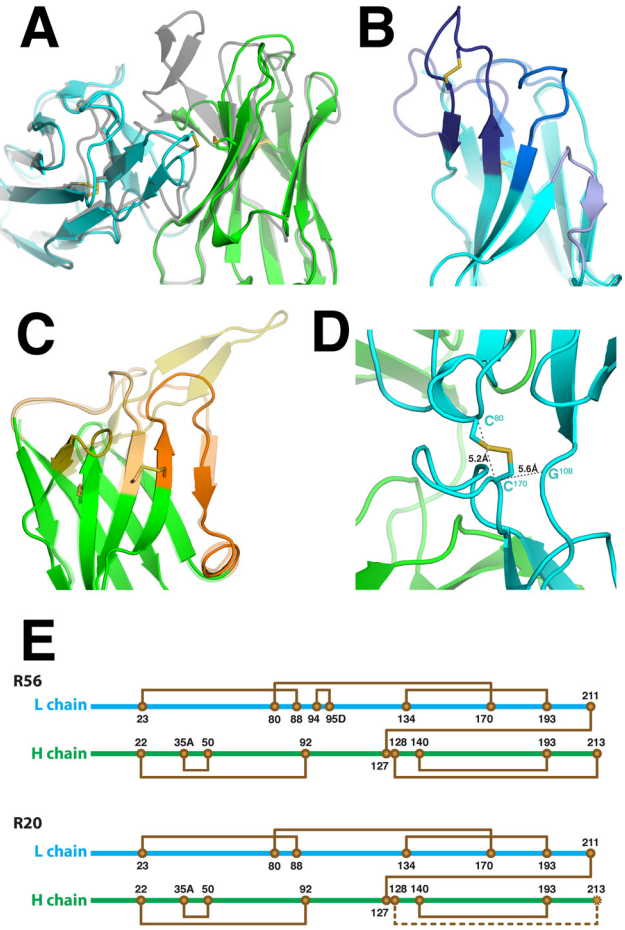

FIG 4 Structural comparison of rabbit MAbs R56 and R20. (A) Superimposition of the Fv regions of R56 (cyan and green) and R20 (gray for both light and heavy chains). The RMSD for superimposition of the C-α atoms is 0.6 Å (195 atom pairs). (B) Superimposition of the light chains of the Fv regions of R56 and R20. The RMSD of the superimposed C-α atoms is 0.4 Å (88 atom pairs). (C) Superimposition of the heavy chains of the Fv regions of R56 and R20. The RMSD for superimposition of the C-α atoms is 0.4 Å (97 atom pairs). (D) Interdomain disulfide bond of the kappa light chain. R56 and R20 both have the disulfide bond between residues L80 and L170. The distance between L108 (Gly in the case of R56 and R20) and L170 is also indicated, as an alternative disulfide bond can form between some of the rabbit kappa light chains. (E) Schematics of the disulfide bonds of R56 and R20. Note that in addition to the interdomain disulfide bond shown in panel D, R56 and R20 have several noncanonical disulfide bonds, including the inter-CDR disulfide bond between residues H35A and H50 in both MAbs and the intra-CDR L3 disulfide bond between L94 and L95D in MAb R56. Dashed lines indicate a potential disulfide bond between residues H128 and H213 of R20 because residue H213 was not visualized in the crystal structure, likely because of the flexibility of the terminal regions.

helical turn (Ile^{P326}, Arg^{P327},and Gln^{P328})—the bend of the fishhook—extends toward the light-chain side of the pedestal. Interestingly, it was previously predicted by sequence analysis that the C-terminal region of V3 has a tendency to form a short alpha helix (52), and it was reported that the V3 C-terminal strand could form a helical conformation in an NMR study of a cyclic V3 peptide (53). However, this region of the full-length V3 structures in the context of the gp120 core does not contain any helical conformation (18, 54). Taken together, these data suggest that this region of V3 is very flexible and it can have many different conformations.

The antigen-antibody interactions buried a total of 804 Å^2 of surface area with 344 Å^2 from the antibody and 460 Å^2 from the epitope. Tyr^{H100G} on the C-terminal strand of the CDR H3 hairpin bisects the antigen-antibody interactions (Fig. 6). The antigen-antibody interactions at the N terminus of the epitope have two components centered at residues Glu^{P322} and Ile^{P322A}, respectively (Fig. 6). First, negatively charged residue Glu^{P322} interacts with Arg^{H54}, forming a hydrogen bond with its amide group. Second, the side chain of hydrophobic residue Ile^{P322A} is buried by the side chains of Tyr^{H52} and Ile^{H56} on one side and by the backbones of Tyr^{H100G} and Ser^{H100H} on the other side. The antigen-antibody interactions at the C terminus of the epitope have three components centered at residues Asp^{P325}, Ile^{P326}, and Arg^{P327}, respectively (Fig. 6). First, Asp^{P325} near the middle of the epitope is buried in the center of the antigen-binding site and its side chain can form hydrogen bonds with the side chains of Ser^{L92} and Tyr^{H100K} and the backbone amide of Ile^{L94}. Second, the side chain of hydrophobic Ile^{P326} is buried by the side chain of Tyr^{L92} on the one side and by the side chains of Val^{H100} and Tyr^{H100G} on the other side. Third, positively charged Arg^{P327} (shaped like the bait on the fishhook) forms a salt bridge with Asp^{L1}, the first residue of the light chain. Three negatively charged residues in the light chain, Asp^{L1}, Glu^{L27}, and Asp^{L95A}, encircle the side chain of Arg^{P327}, holding it at the center of this highly negatively charged environment.

Comparison with the binding modes of mouse and human anti-V3 MAbs. By comparing the antigen-binding mode of R56 with those of all of the available complex structures of anti-V3 MAbs, we found that the antigen-binding mode of mouse MAb 50.1 (IgG2a) is the most similar one (Fig. 7A). Mouse MAb 50.1, although also produced by immunization, was induced by using the disulfide-linked 40-mer cyclic peptide RP70 (INCTRPNYNK RKRIHIGPGR AFYTTKNIIG TIRQAHCNIS), which contains the V3 sequence of strain MN of HIV-1 gp120 (20). The complex structure of MAb 50.1 was resolved to 2.8 Å resolution by cocrystallizing its Fab with another cyclic peptide, MP1 (CKRIHIGPGR AFYTTC) (27). The N-terminal nine amino acids of the peptide were observed in the structure, including the first Cys, a non-HIV-1 amino acid. Only the N-terminal half of the crown hairpin was observed in the 50.1 complex structure, as in the case of R56, although a cyclic peptide was used. Notably, the sequences of the epitopes of MAbs 50.1 and R56 are derived from the same region of the V3 crown, and the structures of the epitopes have the same 3D shape (Fig. 7B), with an RMSD of 0.57 Å for superimposition of the C-α atoms of P305 to P314. The Fv domains of MAbs 50.1 and R56 also superimpose well, with an RMSD of 0.73 Å for the C-α atoms. The details of the antigen-antibody interactions of the two MAbs have several similarities. First, both MAbs have an antigen-binding site shaped like a cradle running along the interface between the light and heavy chains (Fig. 7A). Second, both antigen-binding sites have a hydrophobic base, burying highly conserved Ile^{P307} and Ile^{P309}. Third, MAb 50.1 also harbors Tyr^{L49} in its CDR L2 and stacks Pro^{P313} in the same manner as that of MAb R56.

Some human anti-V3 MAbs also have a binding mode similar to that of R56. The best example is the family of anti-V3 MAbs encoded by IGHV5-51 germ line genes, including MAbs 1006, 2219, 2557, 2558, and 4025 (22, 39). The binding mode of this human MAb family has a couple of similarities to that of R56 and

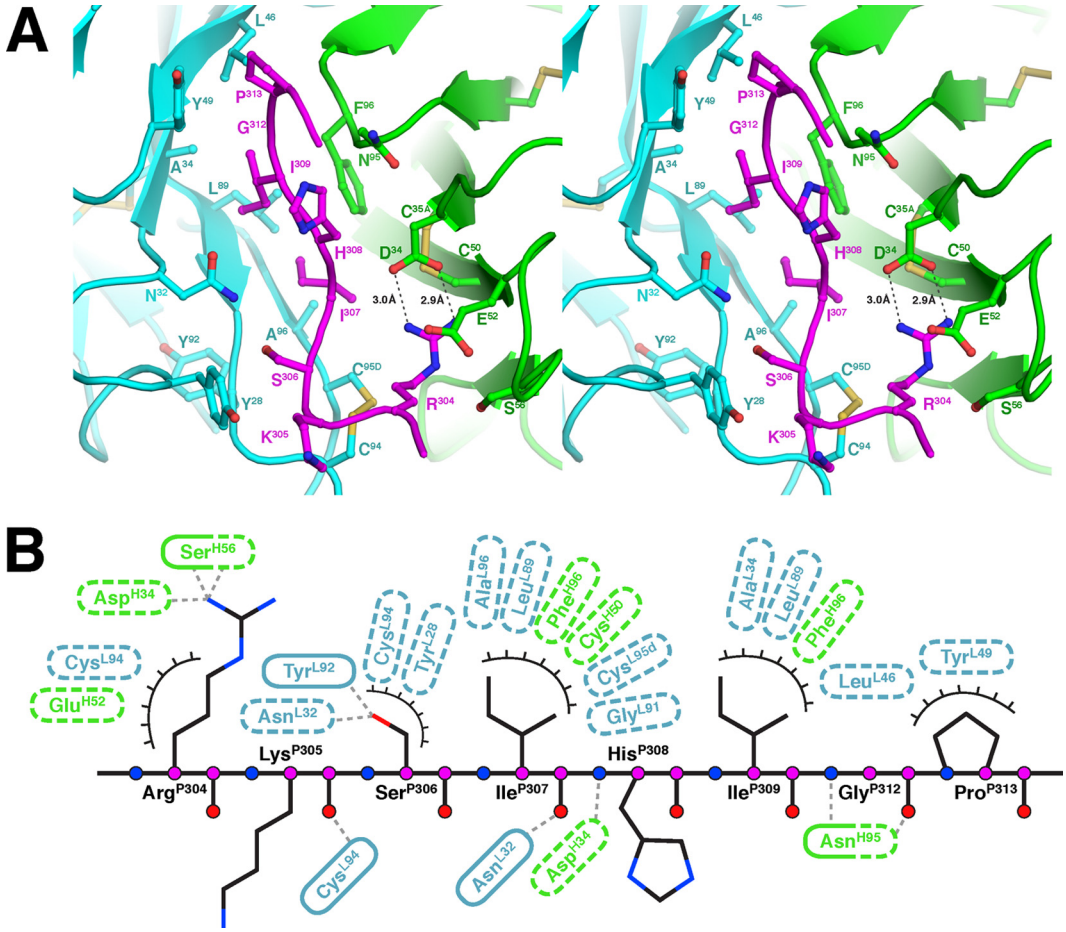

FIG 5 Antigen-antibody interactions in the Fab R56/$V3_{JR-FL}$ complex. (A) Stereo view of the antigen-binding site. Side chains are displayed for key residues involved in the hydrogen bonding and van der Waals interactions (with contact areas greater than 10 $Å^2$). For simplicity, the chain IDs are not shown in residue labels because the chains are already indicated by the coloring scheme. (B) Schematic illustration of antigen-antibody interactions. Hydrogen-binding interactions are indicated by dashed lines between the residues, while van der Waals contacts are indicated by eyelashes. Residues in solid ovals contribute to the interactions by their main chain atoms, and those in dashed ovals contribute by their side chain atoms.

50.1. First, all of these MAbs have a cradle-shaped antigen-binding site with a hydrophobic base that binds conserved N-terminal circlet residues Ile^{P307} and Ile^{P309} of the V3 crown. Structure superimposition showed that the epitope of R56 and the N termini of the epitopes of IGHV5-51 anti-V3 MAbs are very similar; e.g., the structure superimposition of $V3_{JR-FL}$ bound to R56 with the N terminus of $V3_{NY5}$ bound to human MAb 2557 has an RMSD of 1.7 Å (Fig. 7C). Second, Pro^{P313} in the GPG turn of the V3 epitopes bound by the IGHV5-51 anti-V3 MAbs is stacked by a van der Waals interaction against the side chain of a tyrosine (Tyr^{L32}) from the CDR L1 region (19), although in the case of R56, Pro^{P313} is packed against a tyrosine from the CDR L2 region, Tyr^{L49}. However, the binding mode of the human IGHV5-51 anti-V3 MAbs also has a couple of differences from that of MAbs R56 and 50.1. First, the whole beta hairpin of the V3 crown is visible in all of the Fab/epitope complex structures of human IGHV5-51 MAbs, while only the N-terminal half of the V3 crown hairpin could be observed in the complex structures of R56 and 50.1. The C-terminal half of the V3 crown hairpin was also observed in the complex structure of mouse MAb 0.5β determined by an NMR study (55). Interestingly MAb 0.5β was raised by immunization of IIIB gp120, which is different from mouse MAb 50.1, which was raised by a cyclic peptide. Thus, gp120 itself may be able to elicit in mice antibody responses with a more complex epitope. Second, the orientation of the antigen-binding cradle of the IGHV5-51 MAbs is perpendicular to that of R56 and 50.1. In the human case, the epitope bridges the two chains, with the arch of the V3 crown binding the light chain and the band binding the heavy chain (Fig. 7D and E).

The recently identified highly potent human MAb PGT128 has an epitope region that overlaps that of R20. PGT128 binds the mannose glycans harbored by two glycosylation sites (Asn^{P301} and Asn^{P332}) at the base of V3 (40). It also engages amino acids in the C-terminal region of V3 through its CDR H3 by a beta-sheet-type interaction. The key interacting V3 amino acids are residues P323 to P327 (IGDIR), which are at the core of the R20 epitope. Nevertheless, the conformation of the PGT128 epitope is rather different from that of the R20 epitope, reflecting the flexibility of the V3 stem. Interestingly, PGT128 also has a noncanonical disulfide bond between CDRs H1 and H2 that plays a critical role in antigen binding; removing it will make PGT128 lose its gp120-binding activity (40).

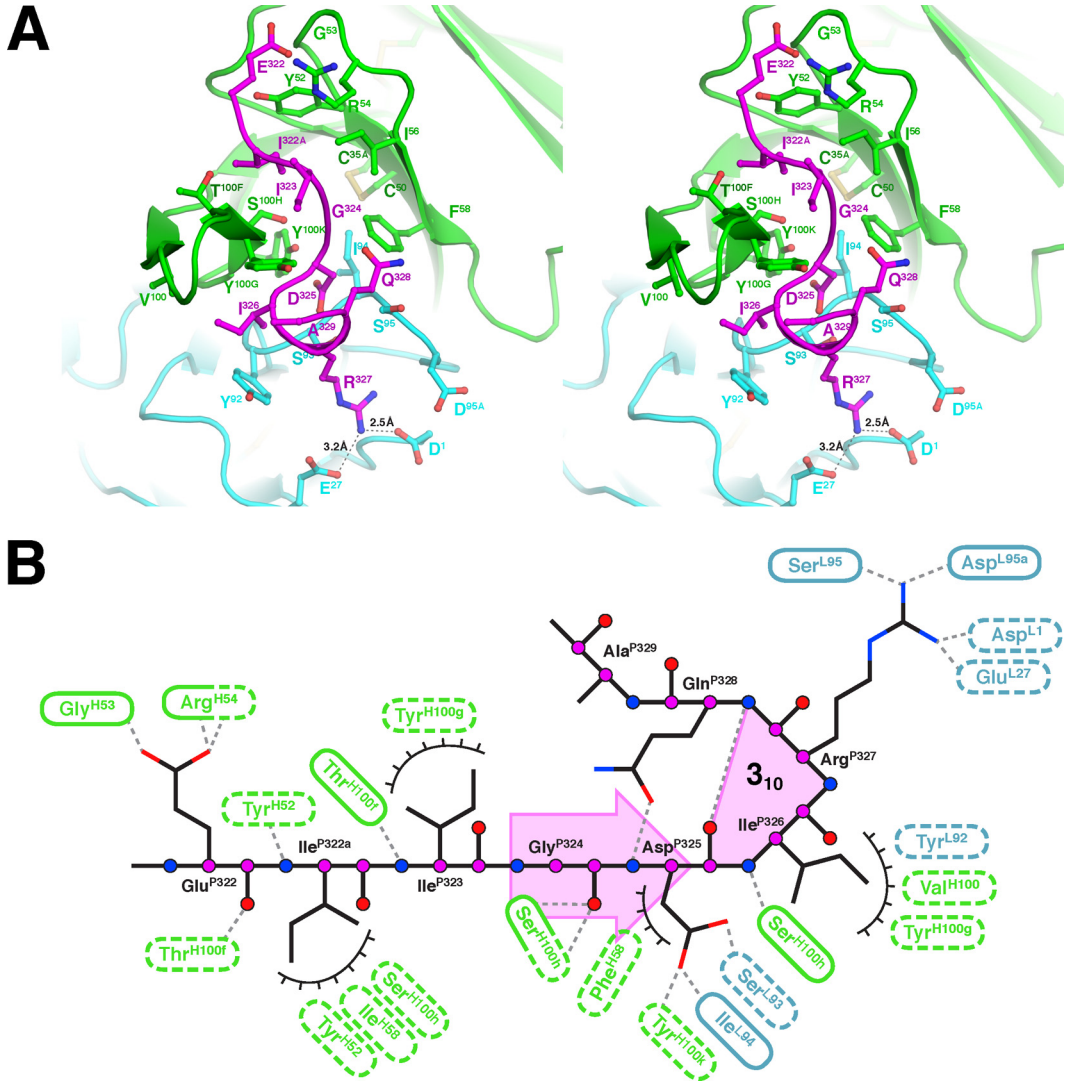

FIG 6 Antigen-antibody interactions in the Fab R20/V3$_{conB}$ complex. (A) Stereo view of the antigen-binding site. Side chains are displayed for key residues. (B) Schematic illustration of the antigen-antibody interactions. The short beta strand in the epitope is indicated by a pink arrow, and the short 3_{10} G turn is indicated by a pink shed.

DISCUSSION

We present Fab/epitope complex structures of two rabbit MAbs, R56 and R20, raised by immunization with gp120 of HIV-1 clade B strain JR-FL with a DNA prime-protein boost regimen. These structures show that they recognize two V3 regions known to be immunogenic in humans—the crown located at the apex and the C-terminal region, including residues from both the V3 stem and base regions (56, 57). R56 has a cradle antigen-binding mode similar to that of a panel of human anti-V3 antibodies encoded by IGHV5-51 germ line genes. Antibodies with this binding mode focus their antigen binding on the highly conserved residues at the N terminus of the V3 crown, consistent with their broad antigen-binding activities. Our analyses further support the notion that the V3 crown has a shape that naturally fits the cradle-binding mode of antibodies. Antibodies with this binding mode are preferentially encoded in humans by the IGHV5-51 germ line genes, making it possible to design a vaccine that elicits antibodies encoded by a specific germ line to target the highly immunogenic V3 crown.

R20 recognizes an epitope consisting of amino acids P322 to P329, just preceding the disulfide bond at the V3 base (Cys^{P296}-Cys^{P331}). This region is spatially close to the two highly conserved glycosylation sites (Asn^{P301} and Asn^{P332}) near the V3 base. The glycans harbored by these two sites have been shown to be part of the epitope of hyperpotent human MAb PGT128 and related MAbs (26). There is also a mouse MAb, IIIB-V3-01, generated by immunization with a linear V3 peptide (FVTIGKIGNM RQA HC), with an epitope mapped to the V3 C-terminal sequence IGKIGNMRQ (25). Unlike PGT128, which has broadly potent neutralization activity, R20 does not neutralize the strains tested (62). There are several potential reasons for this difference. First, the epitope of R20 has a shape very different from that of the V3 region bound by PGT128. Superimposition of the two epitopes showed that only the last five residues of the R20 epitope adopt a

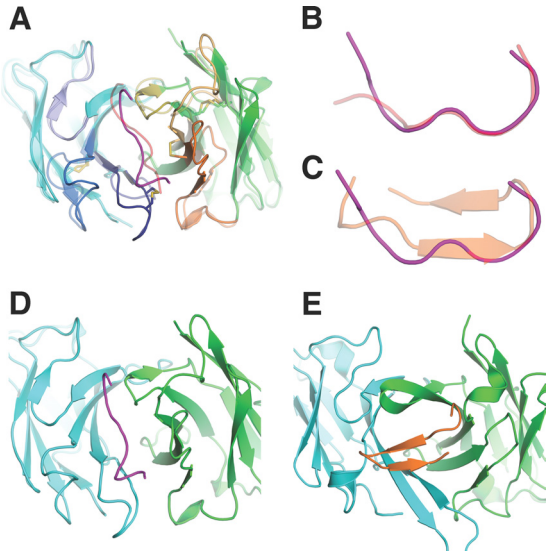

FIG 7 Structural comparison of R56 with mouse and human anti-V3 MAbs. (A) Superimposition of the Fv region of R56 on that of mouse anti-V3 MAb 50.1. The RMSD of the superimposed C-α is 0.73 Å. (B) Superimposition of the $V3_{JR\text{-}FL}$ epitope bound to R56 (magenta) with that bound to mouse MAb 50.1 (salmon). The RMSD of the superimposed C-α of the eight atoms (P305 to P314) is 0.57 Å. (C) Superimposition of $V3_{JR\text{-}FL}$ (magenta) bound to R56 with $V3_{NY5}$ (orange) bound to human MAb 2557. The RMSD of the superimposed 10 C-α atoms (P303 to P314) is 1.7 Å. The antigen-binding modes of MAb R56 and human IGHV5-51 MAb 2557 are shown in panels D and E, respectively.

conformation similar to that of the PGT128 epitope. Second, the epitope of PGT128 consists mainly of glycans harbored by N301 and N332 while our mutagenesis study suggested that R20 does not need glycan for binding (data not shown). Third, R20 approaches the V3 base from an angle tilted about 20° from that of PGT128; this lower approach angle likely hinders its ability to bind gp120 in the trimeric conformation. Nevertheless, the overlapping of the epitopes of MAbs R20, IIIB-V3-01, and PGT128 suggests that this V3 C-terminal region is immunogenic and a target of first immune responses (57). Structurally designed immunogens that target this V3 C-terminal region may induce precursor antibodies with a potential to mature into antibodies that can recognize the glycans at the V3 base in a way that mimics that of PGT128.

Our study of R56 and R20 revealed several features that are unique to rabbit antibodies. (i) We observed that the commonly occurring kappa chain interdomain disulfide bond between Cys^{L80} and Cys^{L170} is located in the elbow region (see also reference 50). It limits the flexibility of the elbow, hence the flexibility of the Fab region of the antibody. Limiting of flexibility not only can contribute to the stability of rabbit antibodies (1) but may also help to increase their binding affinity, as it reduces the entropy of the antibodies. (ii) In addition to this interdomain disulfide bond, we have also observed several noncanonical disulfide bonds among the CDR loops. It is known that noncanonical disulfide bonds are found with relatively low frequency in human and primate antibodies but often in those of chickens, camels, etc. (58–61). Formation of the noncanonical disulfide bonds among the CDR loops increases the variability of CDRs (10). Our data showed that these disulfide bonds can be involved in antigen binding, contributing to the affinity of antibodies. (iii) On the basis of our structures, we computationally modeled the other two major heavy-chain allotypes (a1 and a2) of rabbit antibodies and showed that their allotype marker regions have very different electrostatic surface potentials, providing a structural understanding of the differences among these three allotypes (Fig. 3). (iv) It is known that rabbit antibodies have CDR H3s with lengths ranging from 3 to 22 amino acids (Kabat scheme) (5). Here, R56 has a CDR H3 of only 4 amino acids while R20 has one of 21 amino acids. Interestingly both MAbs were generated from the same rabbit by immunization. These data suggested that the rabbit has the potential to produce highly diverse antibodies with a wide range of CDR H3 lengths.

There are clearly differences between the epitopes recognized by the rabbit MAbs raised by immunization and those recognized by human MAbs derived from chronically infected patients. This can best be understood in the case of R56, as we have for comparison many structures of human anti-V3 MAbs with the same antigen-binding mode. Previous structural data showed that the C-terminal residues of the V3 crown are visible in the complex structures of the human anti-V3 MAbs because these residues engage the antibody by specific interactions sufficient to stabilize the C terminus of the V3 crown (19, 35, 39). For rabbit antibody R56, on the contrary, only the N-terminal half of the V3 crown can be observed in the complex structures. Since the V3 crown tends to have a beta hairpin structure, its C-terminal half must be spatially close to the N-terminal half. However, R56 did not develop contacts with the C terminus of the V3 crown or the contacts were not sufficiently strong to stabilize the C-terminal half to be observable in the crystal structure (but may be observable in NMR structures 55). This is also the case for mouse MAb 50.1, which was raised by immunization as well. Thus, we hypothesize that, because of the limited time intervals and insufficient antigen stimulation in immunization, the immunization-derived antibodies do not have the necessary affinity maturation to develop strong contacts with the C terminus of the V3 crown.

Our structural analyses of R56 and R20 show from several aspects the suitability of using the rabbit as an animal model for AIDS vaccine development. First, the rabbit immune system is able to respond to gp120 immunogens and recognizes immunogenic regions similar to those recognized by the human immune system, such as the crown and C-terminal regions of V3. Second, antibodies elicited by gp120 immunogens in rabbits can mimic the binding modes of human antibodies. This is most clear in the case of antibodies that target the V3 crown. Third, rabbits can produce antibodies with CDR H3s with a wide length range, including antibodies with very long CDR H3s, a hallmark increasingly found in potent human MAbs. Fourth, the long CDR H3s of rabbit antibodies can engage antigen through a beta-sheet-type interaction, a feature often observed in human MAbs with long CDR H3s. Taken together, our data show that the rabbit is a useful animal model in which to test immunogens and immunization regimens in AIDS vaccine development.

ACKNOWLEDGMENTS

We thank Mirek Gorny, Susan Zolla-Pazner, and Katherine Knight for useful discussions and staff members at beam line X6A, NSLS, for their help with X-ray diffraction data collection.

This work was supported by NIH grants AI082274, AI082676, AI065250. and AI100151. HIV-1 consensus subtype B Env (15-mer) pep-

tides were obtained through the AIDS Research and Reference Reagent Program, Division of AIDS, NIAID, NIH.

REFERENCES

1. **Mage RG, Lanning D, Knight KL.** 2006. B cell and antibody repertoire development in rabbits: the requirement of gut-associated lymphoid tissues. Dev. Comp. Immunol. **30:**137–153.
2. **Li WH, Gouy M, Sharp PM, O'HUigin C, Yang YW.** 1990. Molecular phylogeny of Rodentia, Lagomorpha, Primates, Artiodactyla, and Carnivora and molecular clocks. Proc. Natl. Acad. Sci. U. S. A. **87:**6703–6707.
3. **Graur D, Duret L, Gouy M.** 1996. Phylogenetic position of the order Lagomorpha (rabbits, hares and allies). Nature **379:**333–335.
4. **Novacek MJ.** 1996. Taxonomy. Where do rabbits and kin fit in? Nature **379:**299–300.
5. **Popkov M, Mage RG, Alexander CB, Thundivalappil S, Barbas CF, III, Rader C.** 2003. Rabbit immune repertoires as sources for therapeutic monoclonal antibodies: the impact of kappa allotype-correlated variation in cysteine content on antibody libraries selected by phage display. J. Mol. Biol. **325:**325–335.
6. **Ros F, Puels J, Reichenberger N, van Schooten W, Buelow R, Platzer J.** 2004. Sequence analysis of 0.5 Mb of the rabbit germline immunoglobulin heavy chain locus. Gene **330:**49–59.
7. **Ros F, Reichenberger N, Dragicevic T, van Schooten WC, Buelow R, Platzer J.** 2005. Sequence analysis of 0.4 megabases of the rabbit germline immunoglobulin kappa1 light chain locus. Anim. Genet. **36:**51–57.
8. **Kwong PD, Mascola JR.** 2012. Human antibodies that neutralize HIV-1: identification, structures, and B cell ontogenies. Immunity **37:**412–425.
9. **Knight KL, Becker RS.** 1990. Molecular basis of the allelic inheritance of rabbit immunoglobulin VH allotypes: implications for the generation of antibody diversity. Cell **60:**963–970.
10. **Sehgal D, Johnson G, Wu TT, Mage RG.** 1999. Generation of the primary antibody repertoire in rabbits: expression of a diverse set of Igk-V genes may compensate for limited combinatorial diversity at the heavy chain locus. Immunogenetics **50:**31–42.
11. **Kabat EA, Wu TT, Perry HM, Gottesman KS.** 1991. Sequences of proteins of immunological interest, 5th ed. National Institutes of Health, Bethesda, MD.
12. **McCartney-Francis N, Skurla RM, Jr, Mage RG, Bernstein KE.** 1984. Kappa-chain allotypes and isotypes in the rabbit: cDNA sequences of clones encoding b9 suggest an evolutionary pathway and possible role of the interdomain disulfide bond in quantitative allotype expression. Proc. Natl. Acad. Sci. U. S. A. **81:**1794–1798.
13. **Steiner LA.** 1985. Immunoglobulin disulfide bridges: theme and variations. Biosci. Rep. **5:**973–989.
14. **McKeating JA, Gow J, Goudsmit J, Pearl LH, Mulder C, Weiss RA.** 1989. Characterization of HIV-1 neutralization escape mutants. AIDS **3:**777–784.
15. **Ivanoff LA, Dubay JW, Morris JF, Roberts SJ, Gutshall L, Sternberg EJ, Hunter E, Matthews TJ, Petteway SR, Jr.** 1992. V3 loop region of the HIV-1 gp120 envelope protein is essential for virus infectivity. Virology **187:**423–432.
16. **Wyatt R, Kwong PD, Desjardins E, Sweet RW, Robinson J, Hendrickson WA, Sodroski JG.** 1998. The antigenic structure of the HIV gp120 envelope glycoprotein. Nature **393:**705–711.
17. **Resch W, Hoffman N, Swanstrom R.** 2001. Improved success of phenotype prediction of the human immunodeficiency virus type 1 from envelope variable loop 3 sequence using neural networks. Virology **288:**51–62.
18. **Huang CC, Tang M, Zhang MY, Majeed S, Montabana E, Stanfield RL, Dimitrov DS, Korber B, Sodroski J, Wilson IA, Wyatt R, Kwong PD.** 2005. Structure of a V3-containing HIV-1 gp120 core. Science **310:**1025–1028.
19. **Jiang X, Burke V, Totrov M, Williams C, Cardozo T, Gorny MK, Zolla-Pazner S, Kong XP.** 2010. Conserved structural elements in the V3 crown of HIV-1 gp120. Nat. Struct. Mol. Biol. **17:**955–961.
20. **White-Scharf ME, Potts BJ, Smith LM, Sokolowski KA, Rusche JR, Silver S.** 1993. Broadly neutralizing monoclonal antibodies to the V3 region of HIV-1 can be elicited by peptide immunization. Virology **192:**197–206.
21. **Gorny M, Zolla-Pazner S.** 2003. Human monoclonal antibodies that neutralize HIV-1, p 37–51. *In* Korber B, Brander C, Haynes BF, Koup RA, Moore JP, Walker B, Watkins DI (ed), HIV immunology and HIV/SIV vaccine databases 2003. Los Alamos National Laboratory, Los Alamos, NM.
22. **Gorny MK, Wang XH, Williams C, Volsky B, Revesz K, Witover B, Burda S, Urbanski M, Nyambi P, Krachmarov C, Pinter A, Zolla-Pazner S, Nadas A.** 2009. Preferential use of the VH5-51 gene segment by the human immune response to code for antibodies against the V3 domain of HIV-1. Mol. Immunol. **46:**917–926.
23. **Scheid JF, Mouquet H, Feldhahn N, Seaman MS, Velinzon K, Pietzsch J, Ott RG, Anthony RM, Zebroski H, Hurley A, Phogat A, Chakrabarti B, Li Y, Connors M, Pereyra F, Walker BD, Wardemann H, Ho D, Wyatt RT, Mascola JR, Ravetch JV, Nussenzweig MC.** 2009. Broad diversity of neutralizing antibodies isolated from memory B cells in HIV-infected individuals. Nature **458:**636–640.
24. **Corti D, Langedijk JP, Hinz A, Seaman MS, Vanzetta F, Fernandez-Rodriguez BM, Silacci C, Pinna D, Jarrossay D, Balla-Jhagjhoorsingh S, Willems B, Zekveld MJ, Dreja H, O'Sullivan E, Pade C, Orkin C, Jeffs SA, Montefiori DC, Davis D, Weissenhorn W, McKnight A, Heeney JL, Sallusto F, Sattentau QJ, Weiss RA, Lanzavecchia A.** 2010. Analysis of memory B cell responses and isolation of novel monoclonal antibodies with neutralizing breadth from HIV-1-infected individuals. PLoS One **5:**e8805. doi:10.1371/journal.pone.0008805.
25. **Laman JD, Schellekens MM, Lewis GK, Moore JP, Matthews TJ, Langedijk JP, Meloen RH, Boersma WJ, Claassen E.** 1993. A hidden region in the third variable domain of HIV-1 IIIB gp120 identified by a monoclonal antibody. AIDS Res. Hum. Retroviruses **9:**605–612.
26. **Walker LM, Huber M, Doores KJ, Falkowska E, Pejchal R, Julien JP, Wang SK, Ramos A, Chan-Hui PY, Moyle M, Mitcham JL, Hammond PW, Olsen OA, Phung P, Fling S, Wong CH, Phogat S, Wrin T, Simek MD, Koff WC, Wilson IA, Burton DR, Poignard P.** 2011. Broad neutralization coverage of HIV by multiple highly potent antibodies. Nature **477:**466–470.
27. **Rini JM, Stanfield RL, Stura EA, Salinas PA, Profy AT, Wilson IA.** 1993. Crystal structure of a human immunodeficiency virus type 1 neutralizing antibody, 50.1, in complex with its V3 loop peptide antigen. Proc. Natl. Acad. Sci. U. S. A. **90:**6325–6329.
28. **Ghiara JB, Stura EA, Stanfield RL, Profy AT, Wilson IA.** 1994. Crystal structure of the principal neutralization site of HIV-1. Science **264:**82–85.
29. **Stanfield R, Cabezas E, Satterthwait A, Stura E, Profy A, Wilson I.** 1999. Dual conformations for the HIV-1 gp120 V3 loop in complexes with different neutralizing Fabs. Structure **7:**131–142.
30. **Sharon M, Kessler N, Levy R, Zolla-Pazner S, Gorlach M, Anglister J.** 2003. Alternative conformations of HIV-1 V3 loops mimic beta hairpins in chemokines, suggesting a mechanism for coreceptor selectivity. Structure **11:**225–236.
31. **Stanfield RL, Ghiara JB, Ollmann Saphire E, Profy AT, Wilson IA.** 2003. Recurring conformation of the human immunodeficiency virus type 1 gp120 V3 loop. Virology **315:**159–173.
32. **Stanfield RL, Gorny MK, Williams C, Zolla-Pazner S, Wilson IA.** 2004. Structural rationale for the broad neutralization of HIV-1 by human monoclonal antibody 447-52D. Structure **12:**193–204.
33. **Rosen O, Chill J, Sharon M, Kessler N, Mester B, Zolla-Pazner S, Anglister J.** 2005. Induced fit in HIV-neutralizing antibody complexes: evidence for alternative conformations of the gp120 V3 loop and the molecular basis for broad neutralization. Biochemistry **44:**7250–7258.
34. **Rosen O, Sharon M, Quadt-Akabayov SR, Anglister J.** 2006. Molecular switch for alternative conformations of the HIV-1 V3 region: implications for phenotype conversion. Proc. Natl. Acad. Sci. U. S. A. **103:**13950–13955.
35. **Stanfield RL, Gorny MK, Zolla-Pazner S, Wilson IA.** 2006. Crystal structures of human immunodeficiency virus type 1 (HIV-1) neutralizing antibody 2219 in complex with three different V3 peptides reveal a new binding mode for HIV-1 cross-reactivity. J. Virol. **80:**6093–6105.
36. **Bell CH, Pantophlet R, Schiefner A, Cavacini LA, Stanfield RL, Burton DR, Wilson IA.** 2008. Structure of antibody F425-B4e8 in complex with a V3 peptide reveals a new binding mode for HIV-1 neutralization. J. Mol. Biol. **375:**969–978.
37. **Dhillon AK, Stanfield RL, Gorny MK, Williams C, Zolla-Pazner S, Wilson IA.** 2008. Structure determination of an anti-HIV-1 Fab 447-52D-peptide complex from an epitaxially twinned data set. Acta Crystallogr. D Biol. Crystallogr. **64:**792–802.
38. **Burke V, Williams C, Sukumaran M, Kim S, Li H, WangX-H, Gorny MK, Zolla-Pazner S, Kong X-P.** 2009. Structural basis of the cross-

reactivity of genetically related human anti-HIV-1 mAbs: implications for design of V3-based immunogens. Structure **17:**1538–1546.
39. **Gorny MK, Sampson J, Li H, Jiang X, Totrov M, Wang XH, Williams C, O'Neal T, Volsky B, Li L, Cardozo T, Nyambi P, Zolla-Pazner S, Kong XP.** 2011. Human anti-V3 HIV-1 monoclonal antibodies encoded by the VH5-51/VL lambda genes define a conserved antigenic structure. PLoS One **6:**e27780. doi:10.1371/journal.pone.0027780.
40. **Pejchal R, Doores KJ, Walker LM, Khayat R, Huang PS, Wang SK, Stanfield RL, Julien JP, Ramos A, Crispin M, Depetris R, Katpally U, Marozsan A, Cupo A, Maloveste S, Liu Y, McBride R, Ito Y, Sanders RW, Ogohara C, Paulson JC, Feizi T, Scanlan CN, Wong CH, Moore JP, Olson WC, Ward AB, Poignard P, Schief WR, Burton DR, Wilson IA.** 2011. A potent and broad neutralizing antibody recognizes and penetrates the HIV glycan shield. Science **334:**1097–1103.
41. **Vaine M, Wang S, Hackett A, Arthos J, Lu S.** 2010. Antibody responses elicited through homologous or heterologous prime-boost DNA and protein vaccinations differ in functional activity and avidity. Vaccine **28:**2999–3007.
42. **Otwinowski Z, Minor W.** 1997. Processing of X-ray diffraction data collected in oscillation mode, p 307–326. *In* Carter CW, Sweet R (ed), Macromolecular crystallography, part A, vol 276. Academic Press, Inc., New York, NY.
43. **Winn MD, Ballard CC, Cowtan KD, Dodson EJ, Emsley P, Evans PR, Keegan RM, Krissinel EB, Leslie AG, McCoy A, McNicholas SJ, Murshudov GN, Pannu NS, Potterton EA, Powell HR, Read RJ, Vagin A, Wilson KS.** 2011. Overview of the CCP4 suite and current developments. Acta Crystallogr. D Biol. Crystallogr. **67:**235–242.
44. **Adams PD, Grosse-Kunstleve RW, Hung LW, Ioerger TR, McCoy AJ, Moriarty NW, Read RJ, Sacchettini JC, Sauter NK, Terwilliger TC.** 2002. PHENIX: building new software for automated crystallographic structure determination. Acta Crystallogr. D Biol. Crystallogr. **58:**1948–1954.
45. **Emsley P, Cowtan K.** 2004. Coot: model-building tools for molecular graphics. Acta Crystallogr. D Biol. Crystallogr. **60:**2126–2132.
46. **Abagyan RA, Totrov M, Kuznetsov D.** 1994. ICM—a new method for protein modeling and design: applications to docking and structure prediction from the distorted native conformation. J. Comput. Chem. **15:**488–506.
47. **DeLano WL.** 2002. The PyMOL user's manual. DeLano Scientific, Palo Alto, CA.
48. **Abhinandan KR, Martin AC.** 2008. Analysis and improvements to Kabat and structurally correct numbering of antibody variable domains. Mol. Immunol. **45:**3832–3839.
49. **Ratner L, Fisher A, Jagodzinski LL, Mitsuya H, Liou RS, Gallo RC, Wong-Staal F.** 1987. Complete nucleotide sequences of functional clones of the AIDS virus. AIDS Res. Hum. Retroviruses **3:**57–69.
50. **Arai H, Glabe C, Luecke H.** 2012. Crystal structure of a conformation-dependent rabbit IgG Fab specific for amyloid prefibrillar oligomers. Biochim. Biophys. Acta **1820:**1908–1914.
51. **Spurrier B, Sampson JM, Totrov M, Li H, O'Neal T, Williams C, Robinson J, Gorny MK, Zolla-Pazner S, Kong XP.** 2011. Structural analysis of human and macaque mAbs 2909 and 2.5B: implications for the configuration of the quaternary neutralizing epitope of HIV-1 gp120. Structure **19:**691–699.
52. **LaRosa GJ, Davide JP, Weinhold K, Waterbury JA, Profy AT, Lewis JA, Langlois AJ, Dreesman GR, Boswell RN, Shadduck P, et al.** 1990. Conserved sequence and structural elements in the HIV-1 principal neutralizing determinant. Science **249:**932–935. (Erratum, **251:**811, 1991.)
53. **Vranken WF, Fant F, Budesinsky M, Borremans FA.** 2001. Conformational model for the consensus V3 loop of the envelope protein gp120 of HIV-1 in a 20% trifluoroethanol/water solution. Eur. J. Biochem. **268:**2620–2628.
54. **Huang CC, Lam SN, Acharya P, Tang M, Xiang SH, Hussan SS, Stanfield RL, Robinson J, Sodroski J, Wilson IA, Wyatt R, Bewley CA, Kwong PD.** 2007. Structures of the CCR5 N terminus and of a tyrosine-sulfated antibody with HIV-1 gp120 and CD4. Science **317:**1930–1934.
55. **Tugarinov V, Zvi A, Levy R, Hayek Y, Matsushita S, Anglister J.** 2000. NMR structure of an anti-gp120 antibody complex with a V3 peptide reveals a surface important for co-receptor binding. Structure **8:**385–395.
56. **Walker LM, Sok D, Nishimura Y, Donau O, Sadjadpour R, Gautam R, Shingai M, Pejchal R, Ramos A, Simek MD, Geng Y, Wilson IA, Poignard P, Martin MA, Burton DR.** 2011. Rapid development of glycan-specific, broad, and potent anti-HIV-1 gp120 neutralizing antibodies in an R5 SIV/HIV chimeric virus infected macaque. Proc. Natl. Acad. Sci. U. S. A. **108:**20125–20129.
57. **Moore PL, Gray ES, Wibmer CK, Bhiman JN, Nonyane M, Sheward DJ, Hermanus T, Bajimaya S, Tumba NL, Abrahams MR, Lambson BE, Ranchobe N, Ping L, Ngandu N, Abdool Karim Q, Abdool Karim SS, Swanstrom RI, Seaman MS, Williamson C, Morris L.** 2012. Evolution of an HIV glycan-dependent broadly neutralizing antibody epitope through immune escape. Nat. Med. **18:**1688–1692.
58. **Raaphorst FM, Raman CS, Nall BT, Teale JM.** 1997. Molecular mechanisms governing reading frame choice of immunoglobulin diversity genes. Immunol. Today **18:**37–43.
59. **Harmsen MM, Ruuls RC, Nijman IJ, Niewold TA, Frenken LG, de Geus B.** 2000. Llama heavy-chain V regions consist of at least four distinct subfamilies revealing novel sequence features. Mol. Immunol. **37:**579–590.
60. **Zemlin M, Klinger M, Link J, Zemlin C, Bauer K, Engler JA, Schroeder HW, Jr, Kirkham PM.** 2003. Expressed murine and human CDR-H3 intervals of equal length exhibit distinct repertoires that differ in their amino acid composition and predicted range of structures. J. Mol. Biol. **334:**733–749.
61. **Wu L, Oficjalska K, Lambert M, Fennell BJ, Darmanin-Sheehan A, Ni Shuilleabhain D, Autin B, Cummins E, Tchistiakova L, Bloom L, Paulsen J, Gill D, Cunningham O, Finlay WJ.** 2012. Fundamental characteristics of the immunoglobulin VH repertoire of chickens in comparison with those of humans, mice, and camelids. J. Immunol. **188:**322–333.
62. **Chen Y, Vaine M, Wallace A, Han D, Wan S, Seaman M, Montefiori D, Wang S, Lu S.** 2013. A novel rabbit monoclonal antibody platform to dissect the diverse repertoire of antibody epitopes for HIV-1 Env immunogen design. J. Virol. **87:**10232–10243.